Electronic Supplementary Information

Resonant Cavity-enhanced Colloidal Quantum-dot Dual-band Infrared Photodetectors

Yuning Luo, [a,b] *Shuo Zhang,* [a,b] *Xin Tang** [a,b,c] *and Menglu Chen** [a,b,c]

[a.] School of Optics and Photonics, Beijing Institute of Technology, Beijing, China.

[b.] Beijing Key Laboratory for Precision Optoelectronic Measurement Instrument and Technology, Beijing, China.

[c.] Yangtze Delta Region Academy of Beijing Institute of Technology, China.

List of Supplementary Information:

1. Details for absorption simulation

The spectral absorption of HgTe CQDs film is simulated by using COMSOL Multiphysics. By creating 2dimension geometry and setting boundary condition as periodicity, the simulated absorption of HgTe can be obtained as shown in Fig.2b, c. The thickness and index of refraction of the HgTe CQDs is set to be 300 nm and 2.3+0.1i, respectively. Simulated electric field distribution in Fabry-cavity enhanced HgTe CQDs detector is shown in Fig.S1. The low electric filed intensity in QDs section reveals high absorption of HgTe layer. The intensity of the light in a certain band is weakened while the light in another band is enhanced in optical spacer, which proves the potential of spacer in spectral selectivity. By controlling the optical spacer, the spectral interval and width of the enhancement peaks could be tuned, and this feature is useful for multispectral detection to distinguish spectral information.

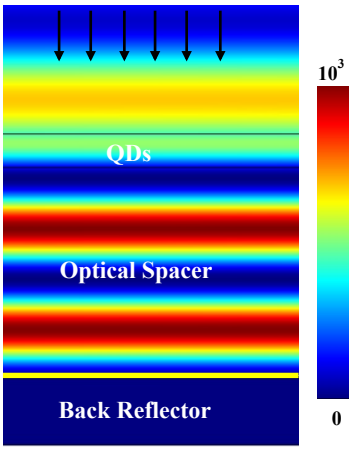

Fig.S1 Simulated light *E*-field mapping in cavity.

2. Bias dependent photo current of MWIR and SWIR ratio

To determine the operation voltages for SWIR mode and MWIR mode, the ratio between the photo current of MWIR and SWIR as a function of bias voltage is calculated, as shown in Fig.S2. The photocurrent I_{ph} can be calculated as:

$$A\int R(\tilde{v})I(\tilde{v})d\tilde{v} = I_{ph}$$

where A is a scaling factor, $R(\tilde{v})$ is the detector relative spectral responsivity, $\tilde{v}$ is the infrared frequency in cm^{-1}, $I(\tilde{v})$ is a known blackbody radiance at 600 °C. With bias voltage $\leq$ -200 mV, $I_{ph\text{-}MWIR}$/ $I_{ph\text{-}SWIR}$ ratio goes to zero, which means the MWIR

photodiode is completely tuned off and the photocurrent is dominated by the SWIR photodiode. In contrast, to turn off the SWIR diode, bias voltage $\geq$ +400 mV is needed.

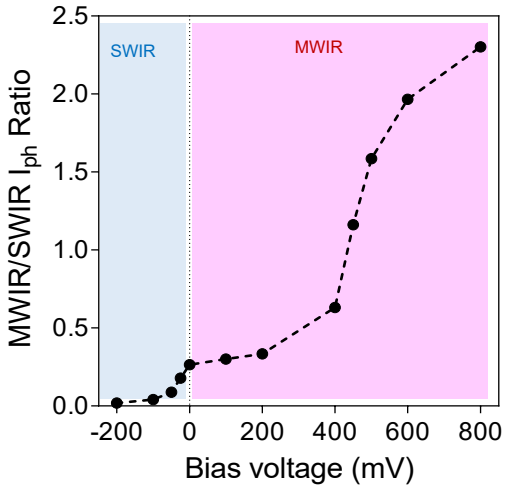

This result shows that the contribution of photocurrent from each diode can be tuned by adjusting the bias voltage.

Fig.S2 The MWIR/SWIR signal ratio as a function of bias voltage.

3. Measurement and calculation of spectral responsivity

The experimental setup of the dual-band detector spectral response is shown in Fig.S3. The spectral response of the dual-band detector is measured with a Fourier-transformed infrared (FTIR) and oscilloscope. The detector is placed within a vacuum-cryostat with controlled temperature. To realize Michelson interferometry measurement with calibrated blackbody as light source, the cryostat is placed on the FTIR, using internal FTIR blackbody as light source. The signal is amplified by a current amplifier at a gain of 10^7 V/A (bandwidth of 500kHz). As movable mirror scans, the signal of interference peak will occur in time domain, as shown in the Fig.S3 inset. The photodetector is located in the position where the interference peak possesses relatively high amplitude. Setting the speed of movable mirror as 0.4747 cm/s, 20-30 sets of data of the interference peak are acquired by oscilloscope. Each of data is processed by Fast Fourier Transform (FFT). Eventually, the spectral response of photodetector can be estimated as shown in Fig. 3b: the wavenumber can be obtained from the ratio between the frequency of FFT result and velocity of movable mirror (0.4747cm/s). The average of the amplitude of each FFT result is calculated as spectral response.

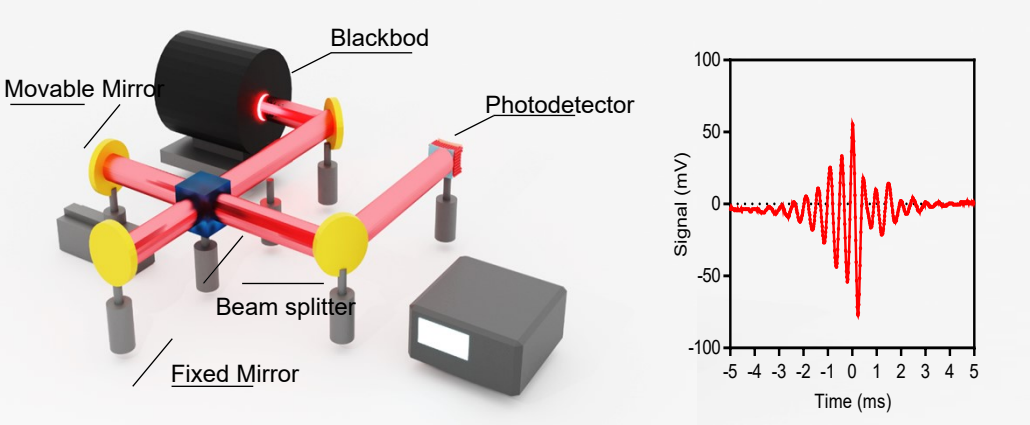

Fig.S3 Experimental setup of the dual-band detector spectral response. The inset is the interference peak captured with oscilloscope.

4. Bias-dependent noise current of dual-band detectors

The noise current in infrared detector mainly includes shot noise, Johnson noise, generation-recombination noise. For the dual-band photodetector, the current is mainly dependent on the shot noise and Johnson noise. The theoretical shot noise can be calculated as

$$i_{shot} = \sqrt{4\, I_d\, e\, \Delta f}$$

where I_d is the dark current, e is the electron charge, Δf is the bandwidth.

The theoretical Johnson noise can be expressed as

$$i_{Johnson} = \sqrt{\frac{4\, k\, T\, \Delta f}{R}}$$

where k is the Boltzmann constant, T is the temperature in kelvin. The noise current is dominated by shot noise while applying bias voltage. In contrast, Johnson noise dominates with zero bias. For example, at 80K, the photodetector has a shunt resistant of 71428.6 and 133333 ohms measured at +0.8V and -0.2V, and the corresponding Johnson noise is 2.5×10^{-13} and 1.8×10^{-13} A/Hz$^{0.5}$ respectively. While the corresponding shot noise is 8.6×10^{-12} and 3.0×10^{-12} A/Hz$^{0.5}$ respectively, which is more than 10 times higher of the Johnson noise. Conversely, at 80K, the shot noise and Johnson noise are 2.5×10^{-14} and 1.8×10^{-13} A/Hz$^{0.5}$ respectively, Johnson noise is about 6 times higher than shot noise. In our experiment, we find that the actual noise is 1-4 times of the theoretical noise.

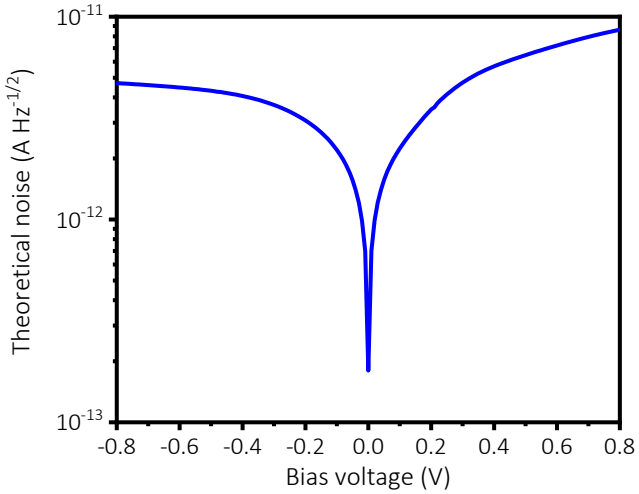

Fig.S4 Theoretical noise of the photodetector as the function of bias voltage

5. Bias-dependent D* of dual-band detectors

The bias-dependent detectivity at 80K for SWIR and MWIR is evaluated (Fig. S5). As forward bias increases, SWIR photodiode will be gradually turned off, the detectivity of MWIR mode will increase. With the reverse bias increasing, SWIR mode slightly decreases due to the increased noise from the dark current. Overall, D* above 10^{10} Jones is achieved for both SWIR and MWIR detector, the peak of the detectivity can reach 1.8×10^{10} and 2.0×10^{10} Jones in SWIR and MWIR mode, respectively.

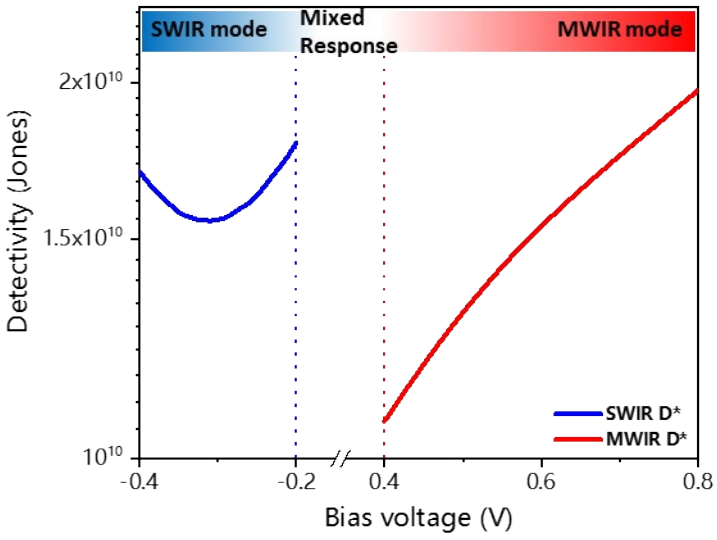

Fig.S5 Detectivity of MWIR mode and SWIR mode as the function of bias voltage

6. Optimization of the thickness of optical spacer

The total spectral responsivity of the photodetector with different spacer thickness is shown in Fig.S6. It is worth noting that the distance of responsivity peak $\Delta\omega$ will vary as space thickness changes, which is highly consistent with the simulation results (Fig.1 b, c). To explore the relationship between $\Delta\omega$ and spacer thickness, the distance of responsivity peak $\Delta\omega$ can be calculated as:

$$\Delta\omega = \frac{1}{2nl_{spacer}}$$

where n is the refractive index of optical spacer, l_{spacer} is the thickness of optical spacer. $\Delta\omega$ can be controlled by changing spacer thickness. For SWIR/MWIR dual-band detector, the responsivity peak may be situated outside the atmospheric and limit practical application when the spacer is excessively thick or thin. Therefore, thickness

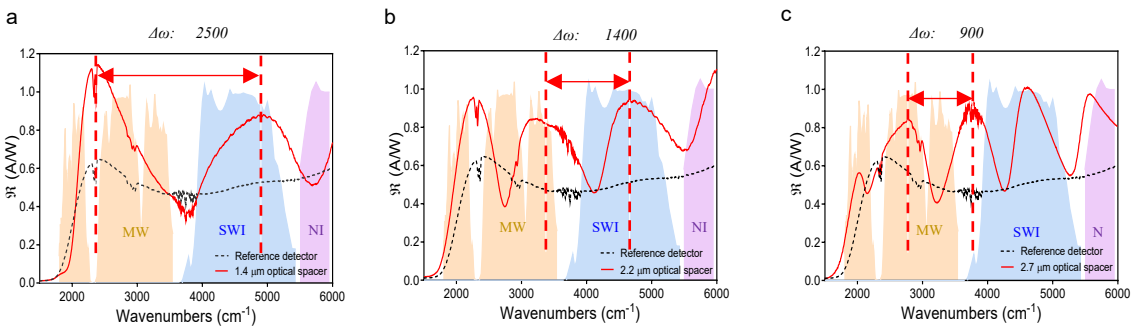

~2μm is an appropriate thickness of our photodetector.

Fig.S6 Overall spectral responsivity of cavity-enhanced dual detector with different spacer thickness (1.4, 2.2 and 2.7μm).

7. Experimental setup for absorption measurement

Fig.S7 shows the design for absorption measurement. The method of measuring background is same to spectral responsivity measurement (Fig.S3). Then, the sample is set between the detector and light source followed by measuring spectral response to get the response of photodetector to the spectrum absorbed by the sample. The transmittance curve be calculated via dividing the spectral response with sample by the background curve.

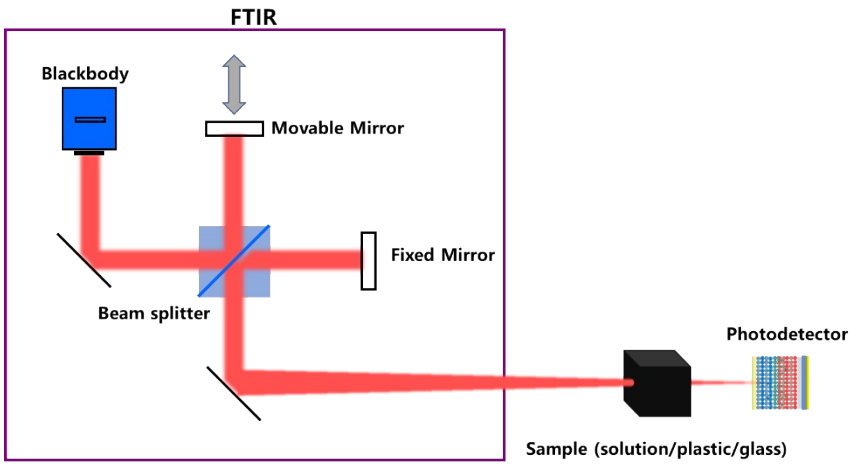

Fig.S7 Experimental setup of the dual-band detector absorption spectrum measurement.

8. Measurement of sample absorption

The samples for absorption measurement captured with visible camera is shown in Fig.S8. The results are shown in Fig.S9. The solution is all transparent and cannot distinguish in visible region. Due to vibrational absorption in SWIR, the transmittance curve of solution is quite different from each other. It is worth noting that the transmittance curve of CBZ looks seem to toluene due to similar chemical constitution. Similarly, same trend can be observed between IPA and ethanol since they are both belong to alcohol. In MWIR region, for the samples made up with polyvinyl chloride (PVC), their absorption curves are quite identical even if their colours are different (black and white). In contrast, although colours are the same, polypropylene (PP) and PVC have distinct transmittance curves: the transmittance curve of PP has the peak at 3600cm^{-1} and transmittance is relatively low at 3250cm^{-1}, this pattern is significantly different from the curve of PVC.

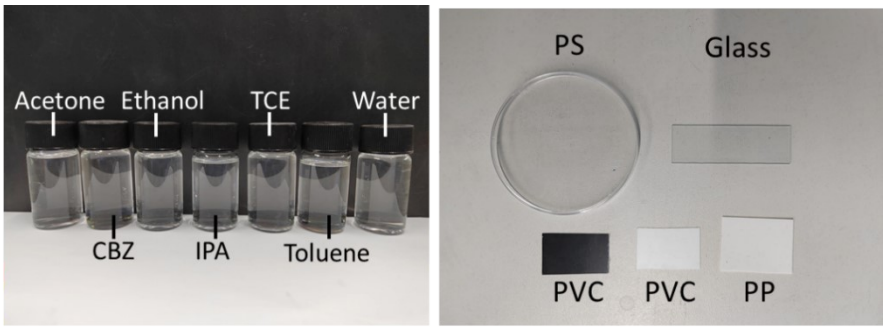

Fig.S8 Different sample for (a) SWIR and (b) MWIR absorption detection captured with visible CMOS camera.

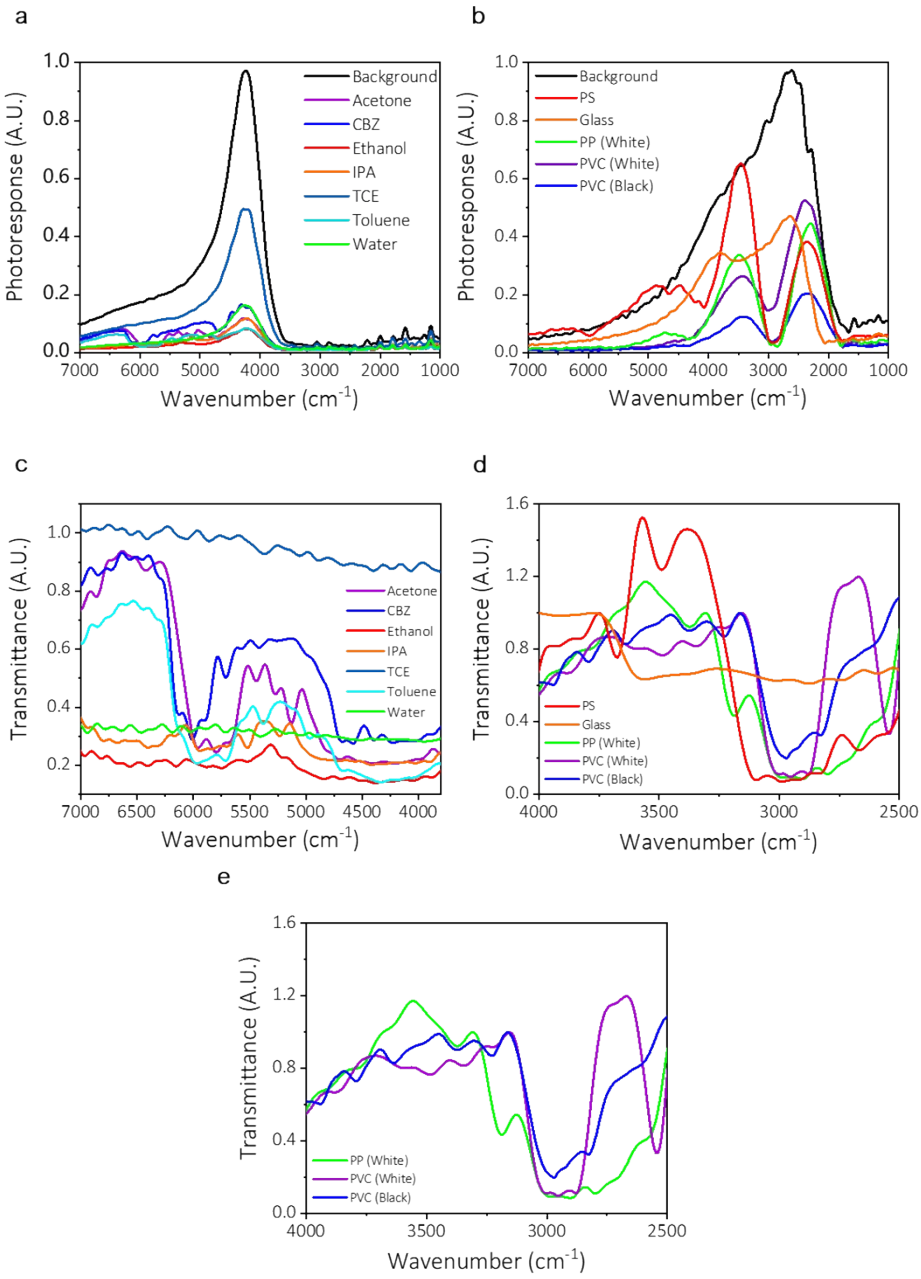

Fig.S9 (a and b) Spectral response with and without sample in SWIR and MWIR mode, respectively. (c and d) Transmittance of samples in SWIR and MWIR mode, respectively. (e) The transmittance of PVC and PP.